Accepted Manuscript

An efficient fourth-order low dispersive finite difference scheme for 2-D acoustic wave equation

Sambit Das, Wenyuan Liao, Anirudh Gupta

PII: S0377-0427(13)00454-8
DOI: http://dx.doi.org/10.1016/j.cam.2013.09.006
Reference: CAM 9320

To appear in: *Journal of Computational and Applied Mathematics*

Received date: 4 September 2012
Revised date: 8 April 2013

Please cite this article as: S. Das, W. Liao, A. Gupta, An efficient fourth-order low dispersive finite difference scheme for 2-D acoustic wave equation, *Journal of Computational and Applied Mathematics* (2013), http://dx.doi.org/10.1016/j.cam.2013.09.006

An efficient fourth-order low dispersive finite difference scheme for 2-D acoustic wave equation

Sambit Das

Department of Mechanical Engineering, IIT Kharagpur, 721302, India

Wenyuan Liao *

Department of Mathematics & Statistics, University of Calgary, Calgary, Alberta, T2N 1N4, Canada

Anirudh Gupta

School of Mechanical and Building Sciences, VIT University, 632014, India

Abstract

In this paper, we propose an efficient fourth-order compact finite difference scheme with low numerical dispersion to solve the two-dimensional acoustic wave equation. Combined with the alternating direction implicit(ADI) technique and Padé approximation, the standard second-order finite difference scheme can be improved to fourth-order and solved as a sequence of one-dimensional problems with high computational efficiency. However such compact higher-order methods suffer from high numerical dispersion. To suppress numerical dispersion, the compact and non-compact stages are interlinked to produce a hybrid scheme, in which the compact stage is based on Padé approximation in both y and temporal dimensions while the non-compact stage is based on Padé approximation in y dimension only. Stability analysis shows that the new scheme is conditionally stable and superior to some existing methods in terms of the Courant-Friedrichs-Lewy (CFL) condition. The dispersion analysis shows that the new scheme has lower numerical dispersion in comparison to the existing compact ADI scheme and the higher-order locally one-dimensional (LOD) scheme. Three numerical examples are solved to demonstrate the accuracy and efficiency of the new method.

Key words: Acoustic Wave Equation, Finite Difference, Padé Approximation, Alternative Direction Implicit, Numerical Dispersion.
PACS: 65M06, 65M32, 65N06

1 Introduction

Numerical solutions of the acoustic wave equations have been widely used in many areas, for example in geophysics, for the purpose of oil exploration, and in medical science, for medical imaging. Among the various numerical methods available, finite difference schemes have attracted the interests of many researchers working on seismic wave propagation (see [12,19,20,22] and references therein) and inverse problems [6,17]. Explicit time-stepping finite difference schemes are very popular in practice due to their ease of implementation [7,12,20], but they usually suffer from moderate to severe stability conditions which only allow very small time step size. The implicit finite difference schemes are more complicated and less efficient in terms of implementation. However such schemes are more stable and allow the use of larger time step size, consequently, are more efficient. Another issue with the numerical simulation of acoustic wave propagation is the numerical dispersion. One remedy is to use highly accurate numerical methods. However it is known that the development of numerical methods with good stability and high accuracy remains a challenging task.

Recently, a great deal of efforts have been devoted to develop higher-order finite difference schemes with low numerical dispersion for the above mentioned acoustic equations and elastic wave equations. For example, in [19], using a plane wave theory and the Taylor series expansion, Liu and Sen proposed a new low dispersive time-space domain finite difference scheme with error of $\mathrm{O}(\tau^2 + h^{2M})$ for 1-D, 2-D and 3-D acoustic wave equations, where τ and h are time step and spatial grid size, respectively, if a $(2M+1)$-point stencil is used for each spatial dimension. It was then shown[20] that, along certain fixed directions the error can be improved to $O(\tau^{2M} + h^{2M})$. In [7], Cohen and Joly extended the works of Dablain [8], Shubin and Bell [24] and Bayliss et al. [2] developed a fourth-order accurate explicit scheme with error of $\mathrm{O}(\tau^4 + h^4)$ to solve the heterogeneous acoustic wave equation. Chu and Stoffa[4] proposed a new implicit finite-difference method which combines a three-level implicit splitting time integration method in time and implicit finite-difference operators of arbitrary order in space. In [30], Yang etc. developed an optimal nearly-analytic discrete to solve the wave equation in 3D anisotropic media. More related works on the accurate and low dispersive numerical methods can be found in [3,21,26,28,29,31–34] and the references therein.

These high order methods are accurate but result in non-compact schemes, which give rise to two issues: efficiency and difficulty in boundary condition treatment. To resolve these issues, many researchers have developed a variety

* Wenyuan Liao
Email address: wliao@math.ucalgary.ca (Wenyuan Liao).

of compact higher-order finite difference schemes to approximate the spatial derivatives. In [5], the authors developed a family of fourth-order three-point combined difference schemes to approximate the first- and second-order spatial derivatives. In [13], the authors introduced a family of three-level implicit finite difference schemes which incorporate the locally one-dimensional method. For more recent compact higher-order difference methods, the readers are referred to [16,18,25,27,35].

Padé approximation based compact higher-order difference scheme works flawlessly for 1D problems, however, for multi-dimensional problems, the difference operator is replaced by a rational function of the finite difference operator, so a block tridiagonal system needs to be solved at each step. To efficiently solve such large linear system, some operator splitting techniques are required to provide efficient boundary treatment and break the multi-dimensional problem down to a number of decoupled one-dimensional problems. Two important operator splitting methods: the alternating direction implicit (ADI) method and the locally one-dimensional (LOD) method are widely used for this purpose. ADI method, which was originally introduced by Peaceman and Rachford [23] to solve parabolic and elliptic equations, has witnessed a lot of development over the years for hyperbolic equations as well [9,14,15]. For example, Fairweather and Mitchell [10] developed a fourth-order compact ADI scheme (THOC-ADI) for solving the wave equation. Recently, locally one-dimensional (LOD) methods have also been found to be very efficient in solving wave equation. Zhang *et al.* [36] have developed a fourth-order compact LOD scheme (HOC-LOD) which has lower dispersion than the typical higher-order compact ADI scheme (THOC-ADI), however it uses an additional intermediate variable although the increase in computational cost and computer memory is marginal.

In this paper, we aim to develop a fourth-order finite difference scheme by integrating Padé approximation in temporal and one spatial dimension and the ADI technique. The resulting scheme is fourth-order in both time and space, and this feature is a perfect fit for hyperbolic-type PDEs such as wave equation, since the CFL condition normally requires that the time step size should be proportional to the spatial step size. Another feature of the new scheme is the flexibility which allows non-compact higher-order approximation of the spatial derivative $\frac{\partial^2 u}{\partial x^2}$ to reduce numerical dispersion.

The rest of the paper is organized as follows. A brief introduction of two existing higher-order splitting schemes is presented in Section 2. A new ADI-based compact finite difference scheme is developed, which is then modified to obtain the new efficient low dispersive scheme in Section 3. The numerical dispersion analysis and stability analysis of the new scheme are conducted in Sections 4 and 5, respectively. We then demonstrate the accuracy and efficiency of the new scheme by applying it to solve three numerical examples in Section 6. Fi-

nally, the conclusions and possible future extensions are addressed in Section 7.

2 Some existing higher-order splitting schemes

In this section we briefly introduce two existing fourth-order compact schemes that have been proposed to solve the 2-D acoustic wave equation in homogeneous media given by

$$\frac{1}{\nu^2}\frac{\partial^2 u}{\partial t^2} = \frac{\partial^2 u}{\partial x^2} + \frac{\partial^2 u}{\partial y^2}, \quad (x, y) \in \Omega \times [0, T], \tag{1}$$

where ν is the wave velocity. The initial conditions are

$$u(x, y, 0) = f_1(x, y), \quad (x, y) \in \Omega, \tag{2}$$
$$u_t(x, y, 0) = f_2(x, y), \quad (x, y) \in \Omega \tag{3}$$

and the boundary condition is defined as

$$u(x, y, t) = g(x, y, t), \quad (x, y, t) \in \partial\Omega \times [0, T]. \tag{4}$$

To simplify the discussion, we assume that $\Omega = [0, 1] \times [0, 1]$, which is divided into a uniform $N_x \times N_y$ grid with equal spatial grid spacing $h_x = 1/(N_x - 1)$, $h_y = 1/(N_y - 1)$, and the grid points are defined as $(x_i, y_j) = ((i - 1)h_x, (j - 1)h_y)$ for $1 \le i \le N_x, 1 \le j \le N_y$. τ denotes the time step size, while $u^n_{i,j}$ denotes the numerical approximation of $u(x_i, y_j, t_n)$. The following acronyms will be used throughout the rest of the paper to simplify the presentation.

- THOC-ADI: Typical higher-order compact alternating direction implicit scheme.
- HOC-LOD: Higher-order compact locally one-dimensional scheme.
- CPD-ADI: Compact Padé approximation based alternating direction implicit scheme.
- NCPD-ADI: Non-compact Padé approximation based alternating direction implicit scheme.
- IPD-ADI: Inter-linked Padé approximation based alternating direction implicit scheme.
- THOM-ADI: Typical higher-order modified alternating direction implicit scheme.

It is well-known [1] that the standard compact central finite difference operators δ_t^2, δ_x^2 and δ_y^2 defined by

$$\frac{\partial^2 u}{\partial t^2}(x_i, y_j, t_n) \approx \frac{\delta_t^2}{\tau^2} u_{i,j}^n = \frac{1}{\tau^2}\left[-2u_{i,j}^n + \left(u_{i,j}^{n-1} + u_{i,j}^{n+1}\right)\right], \tag{5}$$

$$\frac{\partial^2 u}{\partial x^2}(x_i, y_j, t_n) \approx \frac{\delta_x^2}{h_x^2} u_{i,j}^n = \frac{1}{h_x^2}\left[-2u_{i,j}^n + \left(u_{i-1,j}^n + u_{i+1,j}^n\right)\right], \tag{6}$$

$$\frac{\partial^2 u}{\partial y^2}(x_i, y_j, t_n) \approx \frac{\delta_y^2}{h_y^2} u_{i,j}^n = \frac{1}{h_y^2}\left[-2u_{i,j}^n + \left(u_{i,j-1}^n + u_{i,j+1}^n\right)\right] \tag{7}$$

give only second-order approximations to u_{tt}, u_{xx} and u_{yy} at (x_i, y_j, t_n), respectively, where τ is time step, h_x and h_y are grid sizes in x and y directions. To obtain higher-order scheme, one needs to approximate these derivatives with higher-order accuracy.

For comparison, we first introduce a typical higher-order compact ADI scheme (THOC-ADI)[10], which is fourth-order accurate in both time and space. For the simplified case of $h = h_x = h_y$, it is defined as

$$\begin{aligned}\left(1 + \frac{1-r^2}{12}\delta_x^2\right) u_{i,j}^* &= \left[2 + \frac{1+5r^2}{6}\delta_x^2 - \frac{2(1+r^2)}{1-r^2}\delta_y^2\right] u_{i,j}^n \\ &\quad - \left[1 + \frac{1-r^2}{12}\delta_x^2\right] u_{i,j}^{n-1}, \\ \left(1 + \frac{1-r^2}{12}\delta_y^2\right) u_{i,j}^{n+1} &= u_{i,j}^* + \frac{1-r^2}{12}\delta_y^2\left[\frac{2(1+10r^2+r^4)}{(1-r^2)^2} u_{i,j}^n - u_{i,j}^{n-1}\right],\end{aligned} \tag{8}$$

where $r = \frac{v\tau}{h}$ is the CFL number, and $u_{i,j}^*$ is an intermediate solution defined at some time level $t^* \in (t_n, t_{n+1})$. Note here the time level t^* is usually unknown and also no need to be specified.

The second scheme [36] is a fourth-order compact LOD scheme (HOC-LOD) with an error of $O(\tau^4 + h^4)$, which involves the following three stages:

$$(b + r^2 c_2 \delta_x^2) u_{i,j}^n + (a + r^2 c_3 \delta_x^2) u_{i,j}^{n-1} = (a + b + r^2 c_1 \delta_x^2) u_{i,j}^{n-1+s}, \tag{9}$$

$$(a + r^2 \acute{c}_3 \delta_y^2) u_{i,j}^{n+s} + (b + r^2 \acute{c}_3 \delta_y^2) u_{i,j}^{n-1+s} = (a + b + r^2 \acute{c}_1 \delta_y^2) u_{i,j}^n, \tag{10}$$

$$(b + r^2 c_2 \delta_x^2) u_{i,j}^{n+1} + (a + r^2 c_3 \delta_x^2) u_{i,j}^n = (a + b + r^2 c_1 \delta_x^2) u_{i,j}^{n+s}, \tag{11}$$

where $0 < s < 1$ is a parameter. It was shown[36] that to optimize the order of accuracy, $s = \frac{3-\sqrt{3}}{6}$ should be chosen. Other parameters are defined as

$$\begin{aligned}&a = 6 + 2\sqrt{3}, \quad b = 6 - 2\sqrt{3}, \\ &c_1 = \acute{c}_1 = 1 + \frac{1}{r}, \quad c_2 = \acute{c}_2 = \frac{2(1-r)}{ar}, \quad c_3 = \acute{c}_3 = \frac{2(1-r)}{br}.\end{aligned}$$

Note the intermediate value $u_{i,j}^{n-1+s}$ is obtained through solving Eq. (9), which is then used in Eq. (10) to solve for the second intermediate value $u_{i,j}^{n+s}$. Finally the numerical solution $u_{i,j}^{n+1}$ is computed by solving Eq. (11).

Apparently, both schemes are efficient as all linear algebraic equations being solved are tridiagonal systems. However, the second scheme (HOC-LOD) is more expensive and requires more memory since two intermediate values are required at each time step. On the other side, as stated in [36] and also demonstrated in Section 4, the numerical dispersion of HOC-LOD is lower than that of HOC-ADI. Both higher-order compact schemes will be compared with the new scheme in terms of efficiency, accuracy, stability and numerical dispersion.

3 The new higher-order ADI scheme

To develop the new higher-order finite difference scheme we will use two different types of higher-order spatial stencils to approximate the spatial derivatives u_{xx} and u_{yy}.

We first introduce the conventional finite difference spatial stencils which are given in [20] as

$$\frac{\partial^2 u}{\partial x^2}(x_i, y_j, t_n) = \frac{1}{h^2}\left[a_0 u_{i,j}^n + \sum_{m=1}^{M} a_m \left(u_{i-m,j}^n + u_{i+m,j}^n\right)\right] + \mathrm{O}(h^{2M}) \tag{12}$$

$$\frac{\partial^2 u}{\partial y^2}(x_i, y_j, t_n) = \frac{1}{h^2}\left[a_0 u_{i,j}^n + \sum_{m=1}^{M} a_m \left(u_{i,j-m}^n + u_{i,j+m}^n\right)\right] + \mathrm{O}(h^{2M}). \tag{13}$$

Note here for simplicity, we let $h_x = h_y = h$.

Let's denote the non-compact finite difference operators L_x and L_y as

$$\mathrm{L}_x u_{i,j}^n = a_0 u_{i,j}^n + \sum_{m=1}^{M} a_m \left(u_{i-m,j}^n + u_{i+m,j}^n\right), \tag{14}$$

$$\mathrm{L}_y u_{i,j}^n = a_0 u_{i,j}^n + \sum_{m=1}^{M} a_m \left(u_{i,j-m}^n + u_{i,j+m}^n\right), \tag{15}$$

where the coefficients $a_i's$ are obtained by standard Taylor series expansions of Eqs. (12-13). Note that in the conventional finite difference stencils, $M \geq 2$ is required to get fourth-order accuracy in space thus the higher-order conventional finite difference stencils are non-compact in general.

The second type of higher-order spatial stencils are developed by applying the

Padé approximation to the second-order stencils δ_x^2, δ_y^2 and δ_t^2[1,16], which are given as

$$\frac{\delta_x^2}{h^2\left(1+\frac{1}{12}\delta_x^2\right)}u_{i,j}^n = \frac{\partial^2 u}{\partial x^2}(x_i, y_j, t_n) + \mathrm{O}(h^4), \tag{16}$$

$$\frac{\delta_y^2}{h^2\left(1+\frac{1}{12}\delta_y^2\right)}u_{i,j}^n = \frac{\partial^2 u}{\partial y^2}(x_i, y_j, t_n) + \mathrm{O}(h^4), \tag{17}$$

$$\frac{\delta_t^2}{\tau^2\left(1+\frac{1}{12}\delta_t^2\right)}u_{i,j}^n = \frac{\partial^2 u}{\partial t^2}(x_i, y_j, t_n) + \mathrm{O}(\tau^4). \tag{18}$$

Although the conventional finite difference stencils are non-compact they demonstrate lower numerical dispersion. This is because, using compact schemes we cannot increase space stencil greater than 4, but with non-compact scheme, we can take $M > 4$ (see Section 4). So a hybrid scheme will be derived, which consists of conventional higher-order finite difference stencil for interior nodes and compact finite difference stencils for nodes near boundary. In what follows, we describe the two higher-order schemes in detail.

3.1 Higher-order compact ADI scheme

Substituting the fourth-order Padé approximations given in Eqs. (16-18) into the acoustic wave equation Eq. (1) yields

$$\frac{\delta_t^2}{\nu^2\tau^2(1+\frac{1}{12}\delta_t^2)}u_{i,j}^n = \frac{\delta_x^2}{h^2(1+\frac{1}{12}\delta_x^2)}u_{i,j}^n + \frac{\delta_y^2}{h^2(1+\frac{1}{12}\delta_y^2)}u_{i,j}^n + O(\tau^4+h^4). \tag{19}$$

Ignoring the fourth-order error term, and applying $\nu^2\tau^2(1+\frac{1}{12}\delta_t^2)(1+\frac{1}{12}\delta_x^2)(1+\frac{1}{12}\delta_y^2)$ to both sides of Eq. (19) lead to

$$\begin{aligned}&\left(1+\frac{1}{12}\delta_x^2\right)\left(1+\frac{1}{12}\delta_y^2\right)\delta_t^2 u_{i,j}^n = \\ &\quad r^2\left[\left(1+\frac{1}{12}\delta_y^2\right)\left(1+\frac{1}{12}\delta_t^2\right)\delta_x^2 + \left(1+\frac{1}{12}\delta_x^2\right)\left(1+\frac{1}{12}\delta_t^2\right)\delta_y^2\right]u_{i,j}^n,\end{aligned} \tag{20}$$

where $r = \frac{\nu\tau}{h}$.

Collecting terms $\delta_t^2 u_{i,j}^n$ we obtain

$$\left[1+\frac{1-r^2}{12}\delta_x^2+\frac{1-r^2}{12}\delta_y^2+\frac{1-2r^2}{144}\delta_x^2\delta_y^2\right]\delta_t^2 u_{i,j}^n = r^2\left[\delta_x^2+\delta_y^2+\frac{\delta_x^2\delta_y^2}{6}\right]u_{i,j}^n, \tag{21}$$

which is equivalent to

$$\left[1+\frac{1-r^2}{12}\delta_x^2\right]\left[1+\frac{1-r^2}{12}\delta_y^2\right]\delta_t^2 u_{i,j}^n = r^2\left[\delta_x^2+\delta_y^2+\frac{1}{6}\delta_x^2\delta_y^2\right]u_{i,j}^n + Err, \quad (22)$$

where the truncation error term $Err = \frac{r^4}{144}\delta_x^2\delta_y^2\delta_t^2 u_{i,j}^n = O(\tau^6)$, provided that u_{xxyytt} exits and is bounded on $\Omega \times [0,T]$.

Ignoring the truncation error term Err, we obtain the following compact fourth-order numerical scheme

$$\left[1+\frac{1-r^2}{12}\delta_x^2\right]\left[1+\frac{1-r^2}{12}\delta_y^2\right]\delta_t^2 u_{i,j}^n = r^2\left[\delta_x^2+\delta_y^2+\frac{1}{6}\delta_x^2\delta_y^2\right]u_{i,j}^n, \quad (23)$$

which can be efficiently solved in two steps:

$$\left(1-\frac{r^2-1}{12}\delta_x^2\right)\tilde{u}_{i,j} = \left[r^2\delta_x^2+r^2\delta_y^2+\frac{r^2}{6}\delta_x^2\delta_y^2\right]u_{i,j}^n, \quad (24)$$

$$\left(1-\frac{r^2-1}{12}\delta_y^2\right)\delta_t^2 u_{i,j}^n = \tilde{u}_{i,j}, \quad (25)$$

Note that the horizontal boundary conditions $\tilde{u}_{1,j}$ and $\tilde{u}_{N,j}$, $1 < j < N$ are obtained by setting $i = 1$ and $i = N$ in Eq. (25), respectively. Eq. (25) is a three-level scheme that involves solving a tridiagonal system. To see this, we rewrite it in detail as

$$\left(1-\frac{r^2-1}{12}\delta_y^2\right)u_{i,j}^{n+1} = \tilde{u}_{i,j} + \left(1-\frac{r^2-1}{12}\delta_y^2\right)(2u_{i,j}^n - u_{i,j}^{n-1}). \quad (26)$$

The scheme defined in Eqs. (24-25) is compact and fourth-order accurate, and can be solved by ADI technique, so it is referred as CPD-ADI.

3.2 Higher-order interlinked ADI scheme

Despite of its efficiency and accuracy, the compact higher-order finite difference scheme(CPD-ADI) defined in Eqs. (24-25) suffers from moderate numerical dispersion. Actually, it was reported in [20] that the larger number of spatial points been used in Eqs. (12-13), the lower the numerical dispersion will be. We therefore modify this CPD-ADI scheme by replacing the compact Padé approximation based ADI scheme with non-compact higher-order finite difference stencil for interior nodes. More specifically, in the new hybrid ADI

scheme, there are two stages: compact and non-compact stages, which are interlinked and we thereby refer to this new scheme as the interlinked Padé approximation based ADI scheme (IPD-ADI).

In what follows, we describe the new hybrid scheme in detail, with focus on the perspective of implementation. Substituting L_x for the fourth-order difference operator $\frac{\delta_x^2}{1+\frac{1}{12}\delta_x^2}$ in Eq. (19) gives

$$\frac{\delta_t^2}{v^2\tau^2\left(1+\frac{1}{12}\delta_t^2\right)}u_{i,j}^n = \frac{\mathrm{L}_x}{h^2}u_{i,j}^n + \frac{\delta_y^2}{h^2\left(1+\frac{1}{12}\delta_y^2\right)}u_{i,j}^n, \tag{27}$$

which will be used for interior nodes while the ADI scheme in Eq. (19) will be used for nodes near horizontal boundary. To ensure the fourth-order accuracy of the hybrid scheme, the difference between the intermediate values of the two ADI schemes to be interlinked must be of truncation order four or higher. Note in our new hybrid scheme, both stages have the same intermediate values.

Apparently the scheme in Eq. (27) can be interpreted as the result of discretizing the spatial derivatives along y and the temporal derivative Eq. (18) by Padé approximation based higher-order compact scheme and discretizing the spatial derivatives along x by the conventional non-compact higher-order finite difference stencils from Eq. (12). Here we don't use conventional FD stencils in both x and y as the increase in computational cost will be too high to compensate for the decrease in numerical dispersion. Collecting the terms $\delta_t^2 u_{i,j}^n$ leads to

$$\left[1+\frac{1-r^2}{12}\delta_y^2 - \frac{r^2}{12}(1+\frac{1}{12}\delta_y^2)L_x\right]\delta_t^2 u_{i,j}^n = \left[r^2L_x + r^2\delta_y^2 + \frac{r^2}{12}\delta_y^2 L_x\right]u_{i,j}^n, \tag{28}$$

which can be further simplified as

$$\left(1-\frac{r^2}{12}\mathrm{L}_x\right)\left(1-\frac{r^2-1}{12}\delta_y^2\right)\delta_t^2 u_{i,j}^n = \left(r^2\mathrm{L}_x + r^2\delta_y^2\right)u_{i,j}^n + \frac{r^2}{12}\delta_y^2\delta_x^2 u_{i,j}^n. \tag{29}$$

To ensure that the simplified scheme in Eq.(29) is still fourth-order, we need to verify that the difference between Eq. (28) and Eq. (29) is at least fourth-order. Subtracting Eq.(29) from Eq.(28), we can see the difference on the left-hand side is $-\frac{r^4}{144}L_x\delta_y^2\delta_t^2 u_{i,j}^n$, while the difference on the right-hand side is $\frac{r^2}{12}\delta_y^2(\delta_x^2 - L_x)u_{i,j}^n$, hence the total error introduced during the simplification, or in other words, the difference between Eq. (28) and Eq. (29) is

$$\frac{r^4}{144}L_x\delta_y^2\delta_t^2 u_{i,j}^n + \frac{r^2}{12}\delta_y^2(\delta_x^2 - L_x)u_{i,j}^n. \tag{30}$$

If the solution is sufficiently smooth, using Taylor series, one can show that

$$L_x u_{i,j}^n = h^2 u_{xx}(x_i, y_j, t_n) + O(h^{2M}), \quad \delta_x^2 u_{i,j}^n = h^2 u_{xx}(x_i, y_j, t_n) + O(h^4),$$

and

$$\delta_y^2 u_{i,j}^n = h^2 u_{yy}(x_i, y_j, t_n) + O(h^4), \quad \delta_t^2 u_{i,j}^n = \tau^2 u_{tt}(x_i, y_j, t_n) + O(\tau^4),$$

where $M \geq 2$. Since all derivatives are bounded, we can show that

$$L_x \delta_y^2 \delta_t^2 u_{i,j}^n = O(h^4 \tau^2), \quad \delta_y^2(\delta_x^2 - L_x) u_{i,j}^n = O(h^6).$$

Inserting these results into Eq. (30), considering that $r = \frac{\nu\tau}{h}$, we can see the difference between Eq. (28) and Eq. (29) is

$$\begin{aligned}
&\frac{r^4}{144} L_x \delta_y^2 \delta_t^2 u_{i,j}^n + \frac{r^2}{12} \delta_y^2 (\delta_x^2 - L_x) u_{i,j}^n \\
&= \frac{\nu^4 \tau^4}{144 h^4} \cdot O(h^4 \tau^2) + \frac{\nu^2 \tau^2}{12 h^2} \cdot O(h^6) \\
&= O(\tau^6 + \tau^2 h^4),
\end{aligned}$$

which is at least fourth-order in both time and space. We point out here that the reason we substitute δ_x^2 for L_x on the right-hand side of Eq. (29) is to reduce computational cost, as L_x results in a wider stencil.

Similarly, Eq. (29) can be efficiently solved in two steps as

$$\left(1 - \frac{r^2}{12} \mathrm{L}_x\right) u_{i,j}^* = \left(r^2 \mathrm{L}_x + r^2 \delta_y^2\right) u_{i,j}^n + \frac{r^2}{12} \delta_y^2 \delta_x^2 u_{i,j}^n, \tag{31}$$

$$\left(1 - \frac{r^2 - 1}{12} \delta_y^2\right) \delta_t^2 u_{i,j}^n = u_{i,j}^*. \tag{32}$$

In summary, the higher-order non-compact ADI scheme(NCPD-ADI) given in Eqs. (31-32) is used in the non-compact stages for interior nodes while the higher-order compact ADI scheme given in Eqs. (24 -25) will be used in the compact stages for nodes near the horizontal boundary.

We now write the new interlinked Padé approximation based scheme in the decoupled form using intermediate values $\tilde{u}_{i,j}$ and $u_{i,j}^*$. For interior nodes we use the NCPD-ADI scheme

$$\left(1-\frac{r^2}{12}\mathrm{L}_x\right)u^*_{i,j}=\left(r^2\mathrm{L}_x+r^2\delta_y^2\right)u^n_{i,j}+\frac{r^2}{12}\delta_x^2\delta_y^2u^n_{i,j}, \tag{33}$$

$$\left(1-\frac{r^2-1}{12}\delta_y^2\right)\delta_t^2u^n_{i,j}=u^*_{i,j}, \tag{34}$$

while for the nodes near the horizontal boundary we use the following CPD-ADI scheme

$$\left(1-\frac{r^2-1}{12}\delta_x^2\right)\tilde{u}_{i,j}=\left[r^2\delta_x^2+r^2\delta_y^2+\frac{r^2}{6}\delta_x^2\delta_y^2\right]u^n_{i,j}, \tag{35}$$

$$\left(1-\frac{r^2-1}{12}\delta_y^2\right)\delta_t^2u^n_{i,j}=\tilde{u}_{i,j}, \tag{36}$$

where the choice of M in L_x which determines horizontal stencil size is discussed in Section 4.

We outline the main steps of the new higher-order IPD-ADI method as the following(assuming $N_x=N_y=N$):

- Step 1: Compute the initial conditions $u(x_i,y_j,0)$ and $u(x_i,y_j,\tau)$, for $1\leq i,j\leq N$.
- Step 2: Compute the horizontal boundary conditions of $\tilde{u}$ by setting $i=1$ and $i=N$ for $1<j<N$ in Eq. (36).
- Step 3: For $1<j<N$ compute the intermediate variables by solving a sparse linear system, in which the first M equations(for $2\leq i\leq M+1$) and the last M equations(for $N-M\leq i\leq N-1$) are formed using Eq. (35), while the other $N-2M-2$ equations (for $M+1<i<N-M$) are formed using Eq. (33).
- Step 4: Upon the solution of the intermediate variables ($\tilde{u}$ or u^*), solve Eq. (34) or Eq. (36) to compute $u^{n+1}_{i,j}$.
- Step 5: Update the current time level and two initial conditions, and repeat steps 2 - 4 till the final time level reached.

A natural question arises whether the same strategy of using larger spatial finite difference stencils can be applied to the existing schemes to reduce numerical dispersion. Among the higher-order ADI and LOD schemes, ADI schemes are more suitable to implement larger spatial FD stencils because ADI schemes uses less steps than LOD schemes. The increase in computational complexity on implementing larger spatial finite difference stencils for ADI schemes will be much less than that of the LOD schemes. Hence we only present numerical dispersion comparison between the new NCPD-ADI scheme and the THOC-ADI scheme modified by larger spatial finite difference stencils (THOM-ADI) which is obtained using Eq. (8) and Eq. (12) as

$$\left(1+\frac{1-r^2}{12}\mathrm{L}_x\right)u^*_{i,j}=\frac{1-r^2}{12}\mathrm{L}_x\left[\frac{2(1+5r^2)}{(1-r^2)}u^n_{i,j}-u^{n-1}_{i,j}\right]$$
$$2u^n_{i,j}-u^{n-1}_{i,j}-\frac{r^2(1+r^2)}{(1-r^2)}\delta_y^2u^n_{i,j}, \tag{37}$$

$$\left(1+\frac{1-r^2}{12}\delta_y^2\right)u^{n+1}_{i,j}=u^*_{i,j}+\frac{1-r^2}{12}\delta_y^2\left[\frac{2(1+10r^2+r^4)}{(1-r^2)^2}u^n_{i,j}-u^{n-1}_{i,j}\right], \tag{38}$$

and as before with the IPD-ADI scheme, the above scheme is used with the interior nodes only while the original THOC-ADI scheme is used for nodes near the horizontal boundary to preserve the compactness of boundary condition treatment.

3.3 Higher-order approximation of the initial condition

As one can see that both the CPD-ADI scheme and the hybrid scheme IPD-ADI involves a three level scheme which requires two initial conditions to start the computational procedure. In practice, only the first initial condition is explicitly specified. Here we present a fourth-order method to approximate the second initial condition for the three level scheme CPD-ADI given in Eqs. (24-25) and the three level scheme NCPD-ADI given in Eqs. (31-32). To simplify the discussion, we assume that the uniform time step size τ is used. Apparently the first initial condition is explicitly defined as

$$u^1_{i,j}=u(x_i,y_j,0)=f_1(x_i,y_j),\quad 1\le i,j\le N. \tag{39}$$

At a fixed node (x_i,y_j), the function $u(x_i,y_j,t)$ is a single variable function of t. Expanding it by Taylor series at $t=0$, we obtain $u^2_{i,j}$, the fourth-order approximation of $u(x_i,y_j,\tau)$ as

$$\begin{aligned}u^2_{i,j}=&u^1_{i,j}+\tau\frac{\partial u}{\partial t}(x_i,y_j,0)+\frac{\tau^2}{2}\frac{\partial^2u}{\partial t^2}(x_i,y_j,0)+\frac{\tau^3}{6}\frac{\partial^3u}{\partial t^3}(x_i,y_j,0)\\&+\frac{\tau^4}{24}\frac{\partial^4u}{\partial t^4}(x_i,y_j,0)+O(\tau^5)\\=&u^1_{i,j}+\tau f_2(x_i,y_j)+\frac{\nu^2\tau^2}{2}\triangle f_1(x_i,y_j)+\frac{\nu^2\tau^3}{6}\triangle f_2(x_i,y_j)\\&+\frac{\nu^4\tau^4}{24}\triangle^2 f_1(x_i,y_j)+O(\tau^5),\quad 1\le i,j\le N,\end{aligned} \tag{40}$$

provided that $f_1(x,y)$ and $f_2(x,y)$ are sufficiently smooth.

4 Dispersion analysis

Numerical dispersion is the phase error generated when we apply the plane wave theory to the discretized equation with relation to the non-discretized equation. The physical implication of numerical dispersion is the difference in numerical wave speed from the actual wave speed, v. For applying plane wave theory let

$$u_{i,j}^{n} = e^{\mathcal{I}[k\cos\theta(x+ih)+k\sin\theta(y+jh)-\omega(t+n\tau)]}, \quad \mathcal{I} = \sqrt{-1} \in \mathbb{C}, \tag{41}$$

where k is the numerical wave number and θ is the wave propagation angle. For the sake of simplicity we consider $h = h_x = h_y$. Substituting Eq. (41) into Eq. (29) we get the dispersion relation for NCPD-ADI scheme

$$-4\left(1-\frac{r^2}{12}S_1\right)\left(1-\frac{r^2-1}{12}S_3\right)\sin^2\left(\frac{rkh}{2}\right) = r^2S_1 + r^2S_3 + \frac{r^2}{12}S_2S_3, \tag{42}$$

where S_1, S_2, & S_3 are obtained by substituting Eq. (41) into the difference operators L_x, δ_x^2, and δ_y^2, receptively,

$$S_1 = a_0 + 2\sum_{m=1}^{M} a_m\cos(kh\cos\theta), \tag{43}$$

$$S_2 = -4\sin^2\left(\frac{kh\cos\theta}{2}\right), \quad S_3 = -4\sin^2\left(\frac{kh\sin\theta}{2}\right). \tag{44}$$

Similarly the dispersion relation for CPD-ADI scheme can be derived from Eq. (22) as

$$-4\left(1-\frac{r^2-1}{12}S_2\right)\left(1-\frac{r^2-1}{12}S_3\right)\sin^2\left(\frac{rkh}{2}\right) = r^2\left(S_2+S_3+\frac{S_2S_3}{6}\right). \tag{45}$$

For comparison, we derived the dispersion relations for THOC-ADI scheme from Eq. (8) as

$$\begin{aligned}-4\sin^2\left(\frac{rkh}{2}\right) = (S_2+S_3)&\left[\frac{1}{6}(1-r^2)\cos(rkh) - \frac{(1+5r^2)}{6}\right] \\ &+S_2S_3\left[\frac{(1-r^2)^2}{72}\cos(rkh) - \frac{(1+10r^2+r^4)}{72}\right],\end{aligned} \tag{46}$$

and the THOM-ADI scheme from Eq. (38) as

$$-4\sin^2\left(\frac{rkh}{2}\right) = (S_1+S_3)\left[\frac{1}{6}(1-r^2)\cos(rkh) - \frac{(1+5r^2)}{6}\right] + S_1S_3\left[\frac{(1-r^2)^2}{72}\cos(rkh) - \frac{(1+10r^2+r^4)}{72}\right]. \quad (47)$$

The dispersion relation of the HOC-LOD scheme has been derived in [36] and is available therein. Let δ be the normalized phase error given by v_{FD}/v, which is then graphically compared with the exact dispersion relation obtained by substituting Eq. (41) into Eq. (1):

$$\omega^2 = v^2k^2. \quad (48)$$

The normalized phase error is plotted with respect to $0 < kh \leq \pi$, where π is the upper limit at Nyquist frequency. Additionally, we also plot the discrete L_2-norm of deviation of δ from δ_{exact}, which is defined as

$$\|\cdot\|_2 := \frac{1}{P}\left[\sum_{i=1}^{P}\left[\delta(\mathbf{k}[i]h) - \delta_{exact}\right]^2\right]^{\frac{1}{2}}, \quad \mathbf{k} = [k_i]_P, \quad (49)$$

where $P = 100$. Since the analytic representations for dispersion relations are available, instead of using L_2 norm error, we can also use integral average of the error between δ and δ_{exact}, however the plots are the same. The dispersion relations of CPD-ADI, THOC-ADI and HOC-LOD are $\pi/2$ periodic in θ and symmetric about $\pi/4$, which determines the range of their θ variation in Fig. 2. Likewise, the dispersion relation for NCPD-ADI (see Eq. (42)) scheme is π periodic in θ and symmetric about $\pi/2$, so it is plotted for a higher range.

Fig. 1 shows the variation of the numerical dispersion with kh for different numbers of spatial points. It can be observed that if the number of spatial points along one direction increases, there is a decrease in net numerical dispersion in the NCPD-ADI scheme, while the numerical dispersion in the THOM-ADI scheme becomes larger, though for $M = 2$ it demonstrates comparable numerical dispersion. Further, it can be inferred that on increasing M the number of operations for the THOM-ADI scheme grows faster than that of the NCPD-ADI scheme. For example, for $M = 3$, if we compare the number of discrete time and space points needed for computing each time step, it is 15 for THOM-ADI and 13 for NCPD-ADI. Since our aim is to develop schemes with low dispersion, a reasonable increase in computational cost is acceptable, so throughout the rest of the paper, we use $M = 3$ for the NCPD-ADI and IPD-ADI schemes.

To compare the numerical dispersion of the existing and the new schemes, we plotted the normalized phase errors for several propagation angles in Fig. 2. To illustrate the effect of kh and θ, we fixed $r = 0.5$ for all cases. We can see

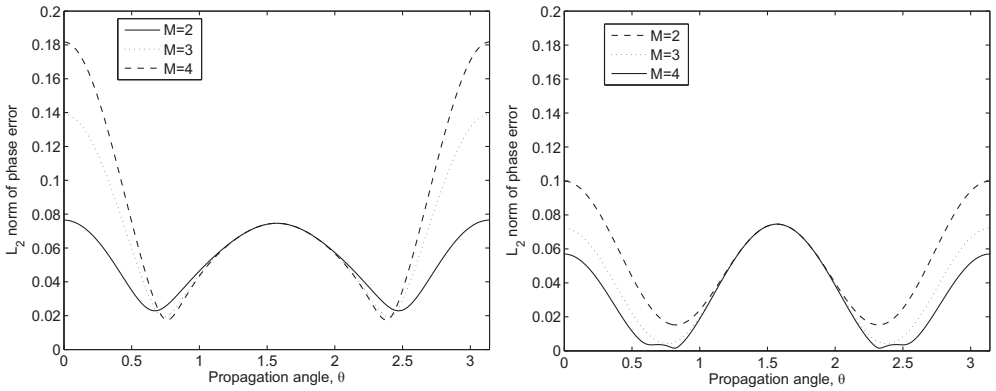

Fig. 1. $\|\delta - \delta_{exact}\|_2$ vs. propagation angles θ for different M, $r = 0.5$. Left: THOM-ADI scheme. Right: NCPD-ADI scheme.

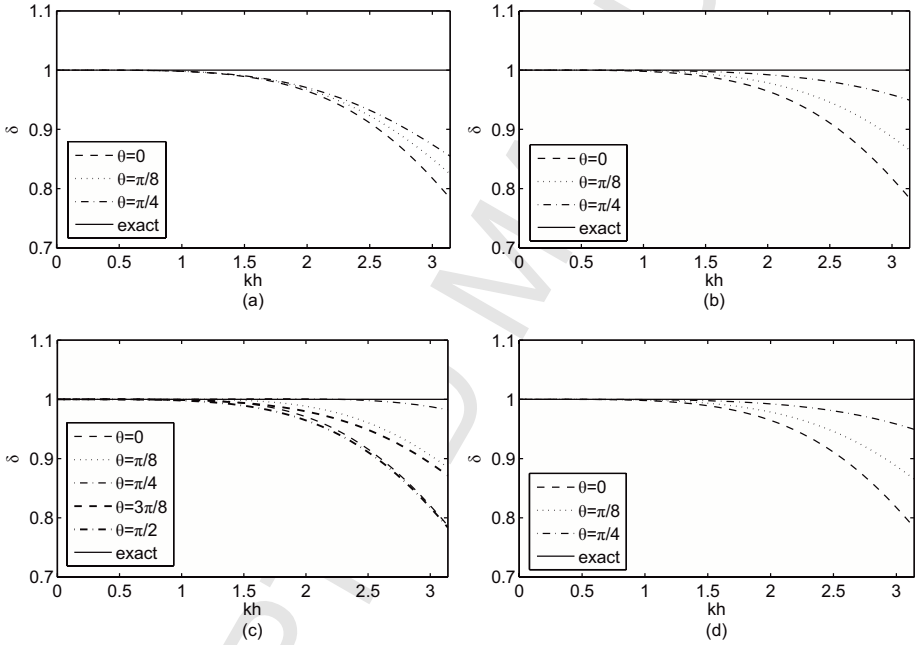

Fig. 2. Normalized phase error for different propagation angles θ, $r = 0.5$. a) THOC-ADI b) HOC-LOD c) NCPD-ADI d) CPD-ADI.

that the numerical dispersions of the HOC-LOD and CPD-ADI schemes are almost identical, and are smaller than that of the THOC-ADI scheme, but are slightly greater than that of the NCPD-ADI scheme. To further show the difference in numerical dispersions, the L_2 norm of the difference $\delta - \delta_{exact}$ for all of the four schemes are plotted in Fig. 3, which confirmed the conclusion drawn from Fig. 2, that is, the numerical dispersion of the new NCPD-ADI scheme is the least among all of the schemes, and the HOC-LOD and CPD-ADI schemes produced similar numerical dispersion which are smaller than

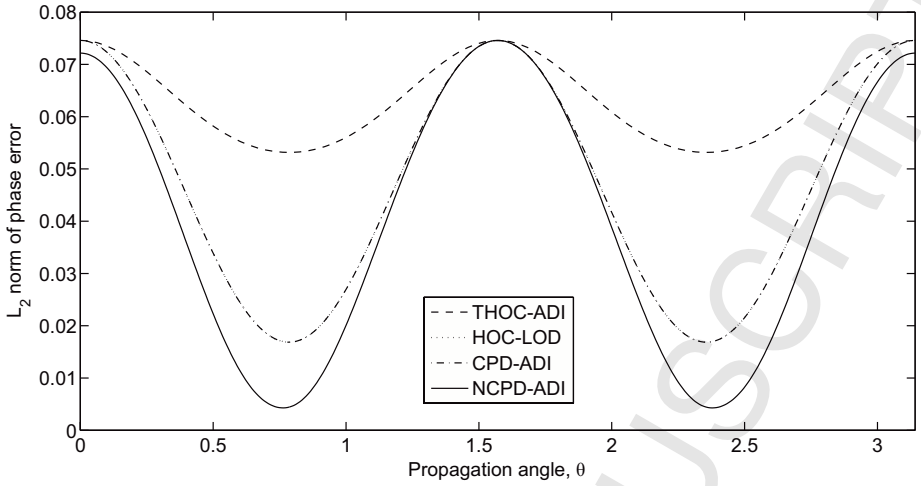

Fig. 3. $\|\delta - \delta_{exact}\|_2$ vs. propagation angle θ, $r = 0.5$.

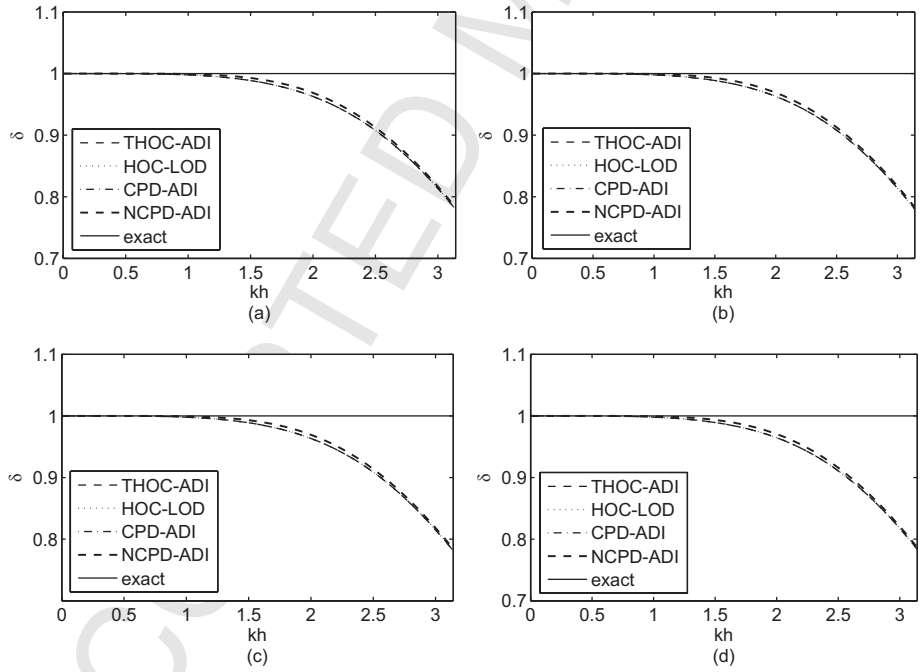

Fig. 4. Normalized phase error for different CFL numbers at propagation angle $\theta = 0$. a) $r = 0.2$ b) $r = 0.3$ c) $r = 0.4$ d) $r = 0.5$.

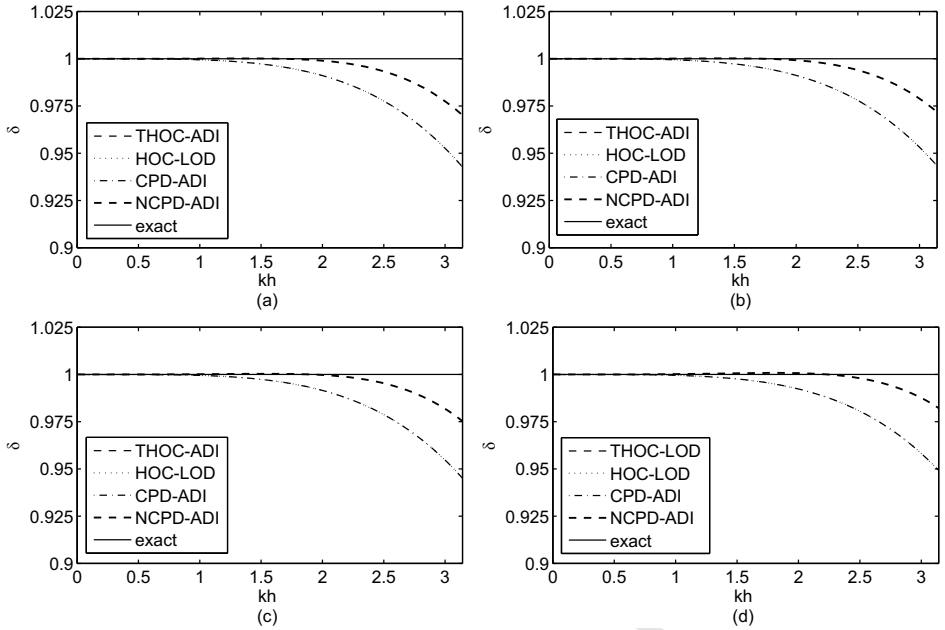

Fig. 5. Normalized phase error for different CFL numbers at propagation angle $\theta = \pi/4$. a) $r = 0.2$ b) $r = 0.3$ c) $r = 0.4$ d) $r = 0.5$.

that of the THOC-ADI, but higher than that of NCPD-ADI. This reconciles with our earlier logic in Section 3, where we used the CPD-ADI scheme just for nodes near the horizontal boundary, so that its effect on the overall numerical dispersion of the IPD-ADI scheme is negligible if a reasonably fine grid is assumed.

To illustrate the effect of CFL number on the numerical dispersion, the normalized phase errors for $r = 0.2$, $r = 0.3$, $r = 0.4$ and $r = 0.5$ are plotted and compared among the four schemes in Fig. 4 for $\theta = 0$, and in Fig. 5 for $\theta = \pi/4$. Interestingly, one can observe that all of the four schemes display similar numerical dispersions, which are not sensitive to the variation of r, However one can still see some difference between the dispersion curves of the new NCPD-ADI scheme and the dispersion curves of the other three schemes, especially when $\theta = \pi/4$. In summary, the NCPD-ADI scheme is better than other existing schemes and CPD-ADI in suppressing numerical dispersion along several propagation angles.

5 Stability analysis

It is known that most of the finite difference schemes used to solve the acoustic wave equation are just conditionally stable and subject to moderate to severe constraints on time step size. Here we analyze the stability of the new schemes

NCPD-ADI and CPD-ADI. using the Von Neumann stability analysis. As we will see later, both new schemes are conditionally stable, however the CFL conditions are different. To make comparison among these schemes, we derive the CFL conditions in the following. For the sake of simplicity, let $h_x = h_y = h$, then $r = \nu\tau/h$ is the CFL number which should satisfy the CFL condition to ensure stability.

Let $u_{i,j}^n = w^n e^{\mathcal{I}[k\cos\theta ih + k\sin\theta jh]}$, then substitute it into the NCPD-ADI scheme Eq. (29), we obtain

$$\begin{aligned}&\left[w^{n+1} - 2w^n + w^{n-1}\right]\left[1 - \frac{(r^2-1)}{12}S_3 - \frac{r^2}{12}S_1 + \frac{r^2(r^2-1)}{144}S_1S_3\right]\\&= w^n\left[r^2S_1 + r^2S_3 + \frac{r^2}{12}S_2S_3\right],\end{aligned}$$

where S_1, S_2 and S_3 are given by Eq. (43). This equation can be rewritten as

$$w^{n+1} = w^n\frac{(2A+B)}{A} - w^{n-1}, \tag{50}$$

where

$$\begin{aligned}A &= \left[1 - \frac{(r^2-1)}{12}S_3 - \frac{r^2}{12}S_1 + \frac{r^2(r^2-1)}{144}S_1S_3\right],\\B &= \left[r^2S_1 + r^2S_3 + \frac{r^2}{12}S_2S_3\right].\end{aligned}$$

Apparently, the characteristic equation of Eq. (50) is

$$P(z) = z^2 - \frac{2A+B}{A}z + 1 = 0. \tag{51}$$

In order for the scheme be stable, the root condition must be satisfied, i.e, we need

$$-2 < \frac{2A+B}{A} < 2 \Longleftrightarrow -4 < \frac{B}{A} < 0. \tag{52}$$

Similarly, for the CPD-ADI scheme, the stability condition is derived as

$$-4 < \frac{\acute{B}}{\acute{A}} < 0, \tag{53}$$

where

$$\acute{A} = \left[1 - \frac{(r_x^2-1)}{12}S_2 - \frac{(r_y^2-1)}{12}S_3 + \frac{(r_x^2-1)(r_y^2-1)}{144}S_2S_3\right],$$
$$\acute{B} = \left[r_x^2 S_2 + r_y^2 S_3 + \frac{r_x^2}{12}S_2S_3 + \frac{r_y^2}{12}S_2S_3\right].$$

For comparison, we list the CFL conditions of the four schemes in Table 1. It

Table 1
CFL conditions for various FD schemes

Scheme	Courant-Friedrichs-Lewy(CFL) condition
THOC-ADI	$\frac{\nu\tau}{h} < 0.7321$
HOC-LOD	$\frac{\nu\tau}{h} < 0.7321$
CPD-ADI	$\frac{\nu\tau}{h} < 0.7657$
NCPD-ADI	$\frac{\nu\tau}{h} < 0.8186$

is shown that the four schemes are comparable in terms of stability, however the new non-compact higher-order method is slightly more stable than others. Here the CFL condition for IPD-ADI has not been derived, but should be between the CPD-ADI and NCPD-ADI.

6 Numerical examples

Three numerical examples are used to demonstrate the efficiency and accuracy of the new higher-order ADI scheme.

6.1 Example 1

We first solve the following initial-boundary value problem on a unit square domain $D = [0,1] \times [0,1]$ to validate the accuracy and efficiency of the new schemes:

$$\begin{aligned} u_{tt} &= u_{xx} + u_{yy}, \quad (x,y,t) \in D \times [0,T], \\ u(x,y,0) &= u_0(x,y), \quad (x,y) \in D, \\ u_t(x,y,0) &= u_1(x,y), \quad (x,y) \in D, \\ u|_{\partial D} &= g(x,y,t), \qquad (x,y,t) \in \partial D \times [0,T], \end{aligned}$$

which has the analytical solution

$$u(x, y, t) = \cos(\sqrt{2}t)\cos(x)\sin(y).$$

To show that the new schemes CPD-ADI and IPD-ADI are fourth-order accurate in space, we fixed $\tau = 0.0025$ so the truncation error from time discretization is negligible, then used various h to solve the example. The L_2 and maximal norms of the errors for both schemes are included in Table 2 and Table 3, respectively, which clearly show that both schemes are fourth-order accurate in space, as the errors are reduced by a factor of 16(roughly) when h is reduced by a factor of 2. It is also clear that IPD-ADI is more accurate than CPD-ADI, as can be seen both the L_2 and Maximum errors of CPD-ADI scheme are about three times of those of the IPD-ADI scheme.

Table 2
L_2 and Maximum errors for **example 1** with $\tau = 0.0025$ at $T = 1$ by the CPD-ADI scheme.

h	1/10	1/20	1/40	1/80
L_2 error: $E_2(h)$	6.2355e-009	4.0810e-010	2.6200e-011	1.7324e-012
$E_2(h)/E_2(h/2)$	-	15.2793	15.5763	15.1235
Conv. Rate	-	3.9335	3.9613	3.9187
Max. error: $E_M(h)$	1.2208e-008	7.7230e-010	4.8443e-11	3.1005e-012
$E_M(h)/E_M(h/2)$	-	15.8073	15.9424	15.6243
Conv. Rate	-	3.9825	3.9948	3.9657

Table 3
L_2 and Maximum errors for **example 1** with $\tau = 0.0025$ at $T = 1$ by the IPD-ADI scheme.

h	1/10	1/20	1/40	1/80
L_2 error: $E_2(h)$	1.9335e-009	1.0217e-010	7.9268e-012	4.6875e-013
$E_2(h)/E_2(h/2)$	-	18.9243	12.8892	16.9105
Conv. Rate	-	4.2422	3.6881	4.0798
Max. error: $E_M(h)$	5.5647e-009	2.3578e-010	1.5475e-11	9.3357e-013
$E_M(h)/E_M(h/2)$	-	23.6012	15.2362	16.5762
Conv. Rate	-	4.5608	3.9294	4.0510

We then show that the two schemes are fourth-order in time as well. Since the schemes are conditionally stable, and the CFL condition must be satisfied, it is impractical to use very small h so that the spatial truncation error can be

ignored. However, we can show the fourth-order accuracy in time by simultaneously reducing h and τ meanwhile maintaining the CFL condition. The order of convergence can be proved by the following contradiction argument. If the scheme is *pth*-order in time, with $p < 4$, halving h and τ several times, the truncation error in time will dominate the total error, thus the total error will be reduced by a factor of $2^p < 16$ when h and τ been halved. In the following numerical test cases, we start from $h = 0.1, \tau = 0.05$, and each time we halve both h and τ. The results for both schemes are included in Table 4 and Table 5, respectively. One can see that the total error is reduced by a factor of 16 (roughly) each time when h and τ are halved, which confirmed that the schemes are fourth-order in time.

Table 4
L_2 and Maximum errors for **example 1** with $h = 2\tau$ at $T = 1$ by the CPD-ADI scheme.

(h, τ)	(1/10,1/20)	(1/20,1/40)	(1/40, 1/80)	(1/80,1/160)
L_2 error: $E_2(h, \tau)$	6.2010e-09	3.7547e-10	2.3054e-11	1.4209e-12
$E_2(h)/E_2(h/2)$	-	16.5153	16.2865	16.2249
Conv. Rate	-	4.0457	4.0256	4.0201
Max. error: $E_M(h)$	1.2256e-08	7.1176e-10	4.2668e-11	2.6009e-12
$E_M(h)/E_M(h/2)$	-	17.2193	16.6814	16.4051
Conv. Rate	-	4.1060	4.0602	4.0361

Table 5
L_2 and Maximum errors for **example 1** with $h = 2\tau$ at $T = 1$ by the IPD-ADI scheme.

(h, τ)	(1/10,1/20)	(1/20,1/40)	(1/40, 1/80)	(1/80,1/160)
L_2 error: $E_2(h, \tau)$	2.1052e-09	1.7894e-10	1.2549e-11	8.1184e-13
$E_2(h)/E_2(h/2)$	-	11.7648	14.2593	15.4575
Conv. Rate	-	3.5564	3.8338	3.9502
Max. error: $E_M(h)$	5.6571e-09	3.9317e-10	2.4064e-11	1.4953e-12
$E_M(h)/E_M(h/2)$	-	14.3884	16.3385	16.0931
Conv. Rate	-	3.8468	4.0302	4.0084

To compare the schemes with other existing schemes in efficiency, we implemented the THOC-ADI scheme [10] and the HOC-LOD scheme [36]. When the same grid and time step are used, the HOC-LOD is the fastest method but it gives the largest error, while the IPD-ADI is the slowest one however it produces the most accurate solution. The CPD-ADI and THOC-ADI are very

Table 6
Efficiency comparison of the four higher-order compact schemes.

Scheme	(h, τ)	L_2 error	Max. error	CPU time(seconds)
HOC-LOD	(1/125, 1/250)	7.1108e-13	1.3062e-12	6.7133
THOC-ADI	(1/125, 1/250)	2.6670e-13	4.8819e-13	7.4863
CPD-ADI	(1/125, 1/250)	2.5308e-13	4.6223e-13	7.7333
IPD-ADI	(1/125, 1/250)	1.3131e-13	2.3947e-13	11.6933

Table 7
Efficiency comparison of the four higher-order compact schemes.

Scheme	(h, τ)	L_2 error	Max. error	CPU time(seconds)
HOC-LOD	(1/125, 1/250)	7.1108e-13	1.3062e-12	6.7133
THOC-ADI	(1/100, 1/200)	6.0369e-13	1.1020e-12	3.713
CPD-ADI	(1/100, 1/200)	5.9484e-13	1.0853e-12	3.8500
IPD-ADI	(1/85, 1/170)	6.2027e-13	1.1425e-12	3.6733

close to each other in terms of both CPU time and accuracy. The results are given in Table 6. In order to make the comparison more sensible, we use the setting for HOC-LOD as the reference, and adjust the grid size h and time step τ for the other three schemes to reach the same error level(roughly), and compare the CPU times. To rule out the effects from some random factors, we ran a large size model, and take the average CPU times of five simulations. The results are included in Table 7, which clearly shows that both CPD-ADI and THOC-ADI comparable in terms of efficiency, while the HOC-LOD is less efficient. Although the IPD-ADI is more efficient than other schemes. However we are aware that the actual results may depend on other factors such as the hardware, software environment and the programming style.

6.2 Example 2

To further confirm the conclusion from the previous example, we solve the second numerical example which is defined as

$$\frac{1}{v^2}\frac{\partial^2 u}{\partial t^2} = \frac{\partial^2 u}{\partial x^2} + \frac{\partial^2 u}{\partial y^2}, \quad (x, y, t) \in [0, 1] \times [0, 1] \times [0, T], \tag{54}$$

where $v = 1$ is the wave propagation velocity. The initial conditions are

$$u(x, y, 0) = \cos(-x - y), \quad \frac{\partial u(x, y, 0)}{\partial t} = -\sqrt{2}\sin(-x - y),$$

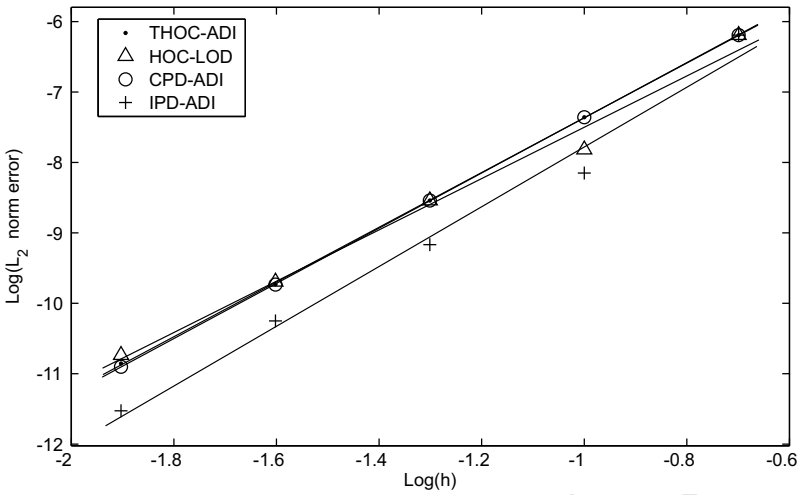

Fig. 6. Log-log plots of L_2-norm errors of the four fourth-order schemes for varying spatial grid size keeping time step size fixed at $\tau = 0.0025$ sec.

while the boundary conditions are chosen accordingly so the analytical solution is

$$u(x, y, t) = \cos\left(\sqrt{2}t - x - y\right).$$

We solve this initial-boundary value problem for $T = 1$, and compute the L_2 norm and maximum norm errors for various spatial and temporal discretizations.

First, the fourth-order accuracy in space is illustrated by using a small time step size τ, combined with various h. The L_2-norm errors are showed in Table 8, which indicates that the scheme IPD-ADI is the most accurate method, while the THOC-ADI, CPD-ADI and HOC-LOD are comparable, although all schemes are fourth-order accurate in space, as indicated from the Log-Log plots of the L_2-norm error in Fig. 6. However, one can see from Table 8 that the convergence rate of HOC-LOD is slightly lower than fourth-order.

We then calculated the maximum errors for each case and the results are included in Table 9 which clearly confirmed that the four schemes are fourth-order in space, as the maximal error for each scheme is reduced by a factor of 16(roughly) when h is halved. It is worthy to point out that, due to the conditional stability, h and τ have to be reduced simultaneously, thus we fix the CFL number r when τ is reduced. The L_2 and maximal errors by various time step size τ are included in Table 10 and Table 11, respectively. One can see that all of the four schemes are fourth-order in time. Additionally, the Log-Log plots of the L_2 norm errors in Fig. 7 also verify that the four schemes are fourth-order in time as well.

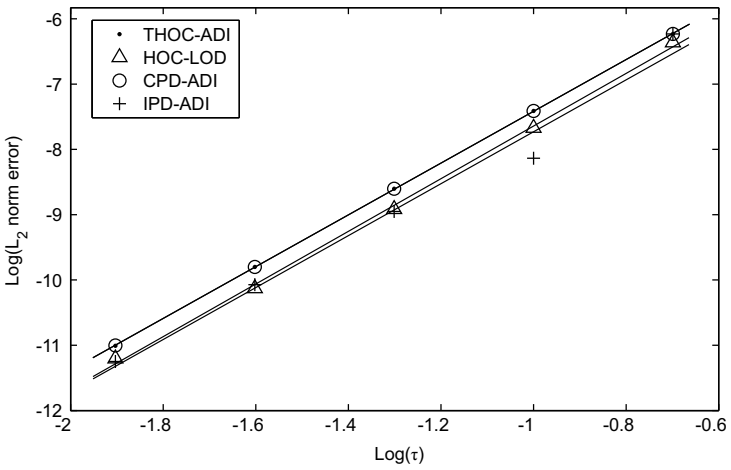

Fig. 7. Log-log plot of L_2-norm errors of the four fourth-order schemes for varying time step sizes keeping the CFL number fixed at $r = 0.5$.

Table 8
L_2 norm errors at $T = 1$ by different schemes with $\tau = 0.0025$ and various h.

$h = h_x = h_y$	THOC-ADI	HOC-LOD	CPD-ADI	IPD-ADI
1/5	6.4455e-07	6.4394e-07	6.4455e-07	6.4455e-07
1/10	4.3974e-008	4.3891e-008	4.3974e-008	7.0756e-009
1/20	2.8785e-009	2.8814e-009	2.8786e-009	6.8012e-010
1/40	1.8559e-010	2.0220e-010	1.8470e-010	5.6304e-011
1/80	1.3959e-011	1.8366e-011	1.2537e-011	2.9731e-012

Table 9
Maximum errors at $T = 1$ by different schemes with $\tau = 0.0025$ and various h.

$h = h_x = h_y$	THOC-ADI	HOC-LOD	CPD-ADI	IPD-ADI
1/5	1.3769e-06	1.3757e-06	1.3769e-06	1.3769e-06
1/10	8.6606e-008	8.6343e-008	8.6608e-008	2.0245e-008
1/20	5.4688e-009	5.4730e-009	5.4690e-009	1.4498e-009
1/40	3.4449e-010	3.7600e-010	3.4277e-010	1.0746e-010
1/80	2.5746e-011	3.4394e-011	2.3074e-011	5.4340e-012

One interesting observation is that, the IPD-ADI scheme shows some inconsistency in error reduction when h and τ are reduced. For example, when (h, τ) is reduced from $(1/5, 1/10)$ to $(1/10, 1/20)$, both L_2 and maximal errors of IPD-ADI shows a convergence order higher than 4. Then, when (h, τ) is further reduced from $(1/10, 1/20)$ to $(1/20, 1/40)$, the IPD-ADI scheme shows

Table 10
Comparison of L_2 norm errors for various temporal discretizations τ with $r = 0.5$.

(h, τ)	THOC-ADI	HOC-LOD	CPD-ADI	IPD-ADI
(1/5, 1/10)	5.8698e-07	4.3402e-07	5.8698e-07	5.8698e-07
(1/10,1/20)	3.8736e-008	2.1267e-008	3.8736e-008	7.3290e-009
(1/20,1/40)	2.4943e-009	1.2133e-009	2.4943e-009	1.1205e-009
(1/40,1/80)	1.5835e-010	7.4417e-011	1.5837e-010	8.4554e-011
(1/80, 1/160)	9.8253e-012	6.2578e-012	9.9039e-012	5.6429e-012

Table 11
Comparison of maximum errors for various temporal discretizations τ with $r = 0.5$.

(h, τ)	THOC-ADI	HOC-LOD	CPD-ADI	IPD-ADI
(1/5, 1/10)	1.2670e-06	9.6829e-07	1.2670e-06	1.2670e-06
(1/10,1/20)	7.6259e-008	4.2143e-008	7.6259e-008	1.8736e-008
(1/20,1/40)	4.7401e-009	2.4180e-009	4.7401e-009	2.3039e-009
(1/40,1/80)	2.9384e-010	1.5111e-010	2.9388e-010	1.5999e-010
(1/80,1/160)	1.8005e-011	1.2392e-011	1.8150e-011	1.0401e-011

an order lower than 4. After that, a consistent fourth-order convergence is observed. Nevertheless, the IPD-ADI is the most accurate method.

6.3 Example 3

To show that the proposed new schemes also work well for a more realist case where a non-zero source term is used to generated the seismic wave, we add a source term to the acoustic wave equation, Eq. (1), which is defined on a square domain $[0, 2400m] \times [0, 2400m]$. Here we use the Ricker's wavelet as the source term, which is given by

$$f(x, y, t) = \delta(x - x_0, y - y_0) \left[1 - 2\{\pi f_p(t - d_r)\}^2\right] e^{-\{\pi f_p(t-d_r)\}^2},$$

where f_p is the peak frequency, d_r is the temporal delay and $\delta(x - x_0, y - y_0)$ is the Dirac delta function centered at x_0, y_0. In this numerical example, we take the peak frequency $f_p = 30$hz, $d_r = 2/f_p$, $x_0 = 1000m, y_0 = 1000m$ and wave velocity $v = 3000m/s$.

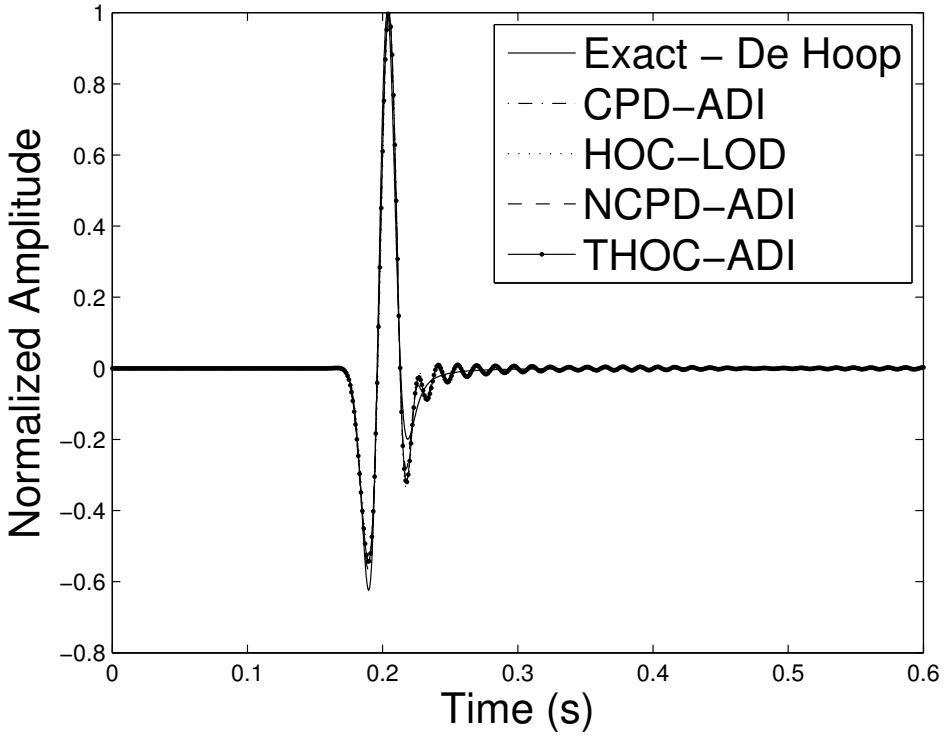

Fig. 8. Normalized waveforms computed by the four schemes with $\tau = 0.002$, $h = 40m$ at the coordinates $(1200m, 1200m)$ and the normalized exact waveform by De Hoop. Wave velocity $v = 3000m/s$. The waveforms are generated by a Ricker wavelet source of 30 hz peak frequency located at $(1000m, 1000m)$.

To avoid boundary reflection, and to better compare the four numerical methods, we run the numerical simulations for $t \in [0, 0.6]$, and generate the exact waveform using the analytic solution given in [11]. Fig. (8) shows the normalized amplitudes of the calculated waveforms and the normalized amplitude of the exact waveform. Clearly all of the four methods produce accurate results. As one can see, when $h = 40m$, there is only slight difference between the exact wave form and the calculated waveform by any of the four methods. However, one can still see that the IPD-ADI scheme is slightly more accurate than the other three methods. We also noticed that the CPD-ADI scheme and THOC-ADI give almost exactly the same results, while the HOC-LOD is a little less accurate than the other three methods, although the difference is small. This observation is consistent to the data in Table 6 for example 2. Fig. (9) shows the comparison when $h = 10m$. Clearly all methods produced very accurate results, since there is no visible difference between the exact solution and computed solutions by the four methods.

To validate the new schemes, we plotted the wavefield snapshots computed by IPD-ADI at $t = 0.2s, 0.4s, 0.5s$ and $0.6s$ in Fig.(10). It is noted that when $h = 10m$, the numerical results generated by the four methods are very close

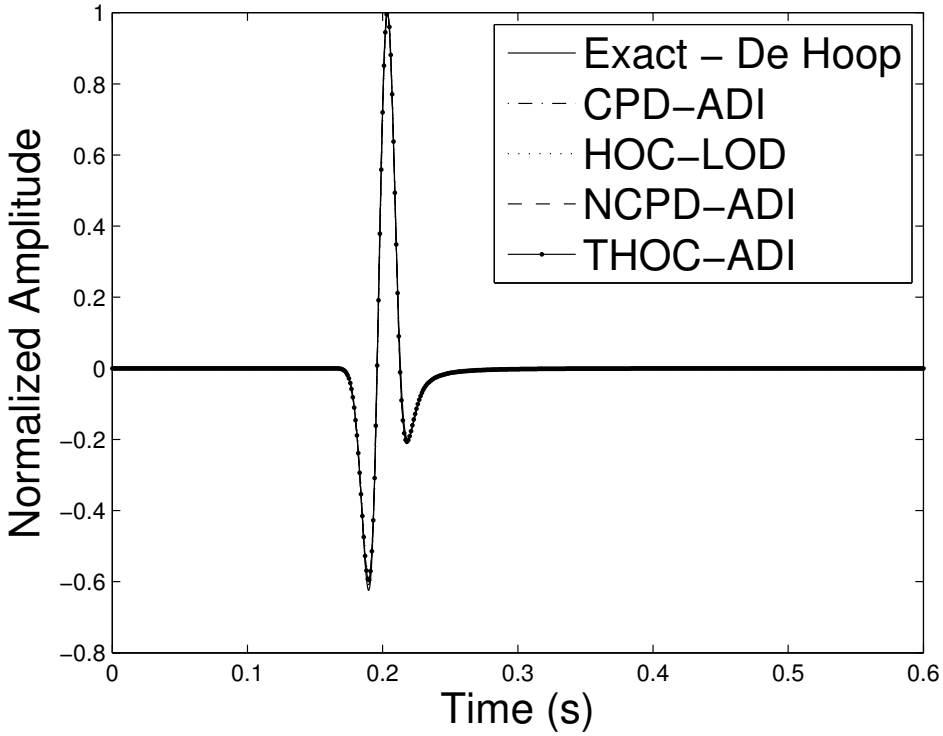

Fig. 9. Normalized waveforms computed by the four schemes with $\tau = 0.001$, $h = 10m$ at the coordinates $(1200m, 1200m)$ and the normalized exact waveform by De Hoop. Wave velocity $v = 3000m/s$. The waveforms are generated by a Ricker wavelet source of 30 hz peak frequency located at $(1000m, 1000m)$.

to each other, so we show the result by IPD-ADI only. One can clearly see the simulated wave propagation is very accurate as the wave front is in a nearly perfect circle shape. When $t = 0.5s$, we can see the wave front arrives the boundary and some reflection can be observed. When $t = 0.6s$, reflections at the four sides of the boundary are clearly shown.

7 Conclusions and future work

We first developed a fourth-order compact ADI finite difference scheme(CPD-ADI) to solve the two-dimensional acoustic wave equation, which is slightly superior to the classical ADI finite difference scheme (THOC-ADI) and comparable to the higher-order compact locally one-dimensional scheme(HOC-LOD). To further improve the method in suppressing numerical dispersion, we then modified CPD-ADI to IPD-ADI scheme. We investigated the feasibility of combining Padé approximation of difference operator with ADI method to obtain higher-order accuracy and efficiency in numerical simulation of wave

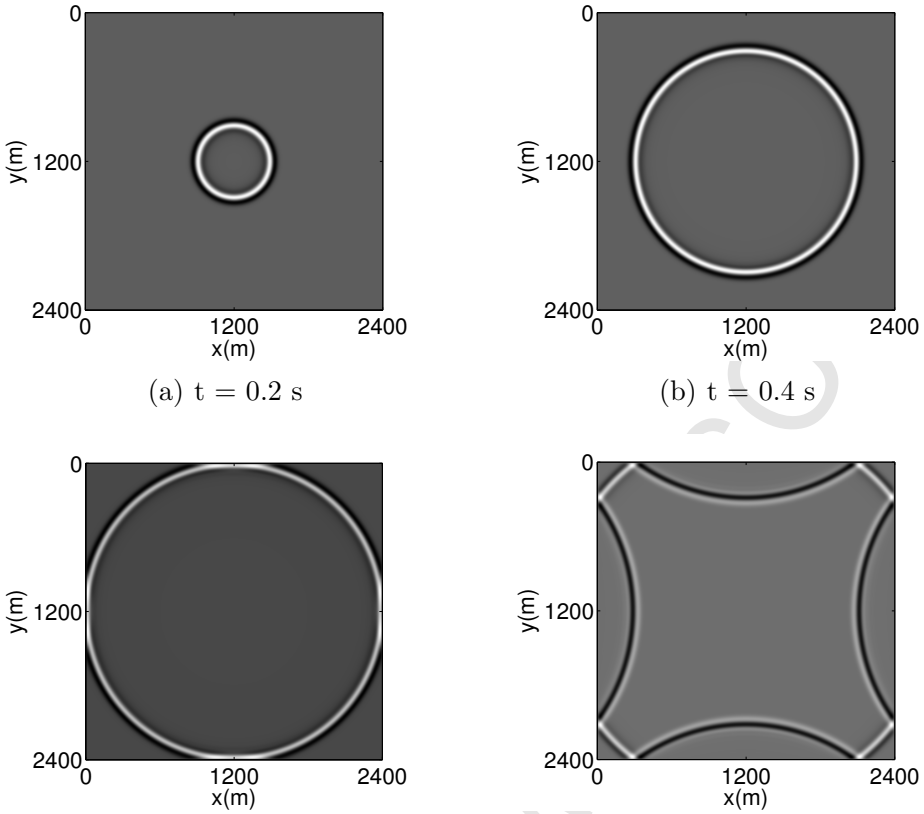

(a) t = 0.2 s (b) t = 0.4 s

(c) t = 0.5 s (d) t = 0.6 s

Fig. 10. Wavefield snapshots at (a) t=0.2s, (b) t = 0.3s, (c) t = 0.4s and (d) t=0.5s.

propagation. The proposed new method(NCPD-ADI) is a three level scheme with error of $O(\tau^4 + h^4)$, which is obtained by applying Padé approximations in both temporal and spatial dimensions. The new scheme is conditionally stable and the CFL condition is superior to that of many other widely used difference methods. This feature is critical for efficiency as it allows the use of larger time step. Numerical results demonstrate that the new scheme NCPD-ADI is more accurate, at the cost of some increase in computational cost, which makes it suitable for efficient and accurate numerical simulation of wave propagation. Meanwhile we noticed that the IPD-ADI's flexibility (due to the variable order M in its non-compact statge) makes it an excellent complimentary scheme to the existing higher-order schemes such as THOC-ADI, HOC-LOD and CPD-ADI. In the future, we plan to extend the method to the acoustic wave equation with variable velocity or elastic wave equations, and three-dimensional problems as well.

Acknowledgments

The work of the first and third authors is supported by MITACS through the Globalink program. The work of the second author is supported by the Natural Sciences & Engineering Research Council of Canada(NSERC) through the individual Discovery Grant program. The authors gratefully acknowledge the financial support from MITACS and NSERC. The authors are grateful for the comments and suggestions from the anonymous reviewers. Their insightful suggestions and comments significantly improved the manuscript, and trigged some possible future work.

References

[1] Y. Adam, Highly accurate compact implicit methods and boundary conditions, Journal of Computational Physics, 24(1977)10–22.

[2] A. Bayliss, K.E. Jordan, B. Lemesurier, E. Turkel, A fourth-order accurate finite difference scheme for the computation of elastic waves, Bull. Seismol. Soc. Amer. 76(4)(1986)1115-1132.

[3] S. Chen, D.H. Yang, X.Y. Deng, A weighted Runge-Kutta method with weak numerical dispersion for solving wave equations, Communications in Computational Physics. 7(5)(2010)1027–1048.

[4] C. Chu, P. Stoffa, Implicit finite-difference simulations of seismic wave propagation, Geophysics, 77(2)(2012)T57–T67.

[5] P. Chu and C. Fan, A three-point combined compact difference scheme, Journal of Computational Physics, 140(1998)370–399.

[6] J.F. Claerbout, Imaging the Earths Interior, Blackwell Scientific Publications Inc., Palo Alto, CA, 1985.

[7] G. Cohen, P. Joly, Construction and analysis of fourth-order finite difference schemes for the acoustic wave equation in non-homogeneous media, SIAM J. Numer. Anal. 4 (1996) 12661302.

[8] M. A. Dablain, The application of high order differencing for the scalar wave equation, Geophysics, 51(1)(1986)54–66.

[9] J. Douglas Jr., J. Gunn, A general formulation of alternating direction methods part I. Parabolic and hyperbolic problems, Numer. Math. 6 (1966)428453.

[10] G. Fairweather, A.R. Mitchell, A high accuracy alternating direction method for the wave equation, J. Inst. Math. Appl. 1 (1965) 309–316.

[11] A T de. Hoop, A modification of Cagniard's method for solving seismic pulse problems. Appl. sci. Res. (section B), 8(1960)349–356.

[12] K.R. Kelly, R.W. Ward, S. Treitel, E.M. Alford, Synthetic seismograms: A finite difference approach, Geophysics 41(1976) 227.

[13] S. Kim, H. Lim, High-order schemes for acoustic waveform simulation, Applied Numerical Mathematics, 57(2007)402-414.

[14] M. Lees, Alternating direction and semi-explicit difference methods for parabolic partial differential equations, Numer. Math. 3 (1961) 398412.

[15] M. Lees, Alternating direction methods for hyperbolic differentials equations, J. Soc. Industrial Appl. Math. 10 (1962) 610–616.

[16] S. K. Lele, Compact finite difference schemes with spectral-like resolution, Journal of Computational Physics 103(1992) 1642.

[17] W. Liao, A computational method to estimate the unknown coefficient in a wave equation using boundary measurements, Inv. Prob. Sci. Engg. 19 (2011) 855–877.

[18] W. Liao, A Compact High-Order Finite Difference Method for Unsteady Convection-Diffusion Equation, Int. J. Comput. Methods Eng. Sci. Mech. 13 (2012)135–145.

[19] Y. Liu, M. K. Sen, An implicit staggered-grid finite-difference method for seismic modelling, Geophys. J. Int. 179 (2009)459–474.

[20] Y. Liu, M. K. Sen, A new timespace domain high-order finite-difference method for the acoustic wave equation, Journal of Computational Physics, 228 (2009) 8779–8806.

[21] X. Ma, D.H. Yang, F.Q. Liu, A nearly-analytic symplectic partitioned Runge-Kutta method for 2D elastic wave equations, Geophysical Journal International, 187(2011) 480–496.

[22] B. G. Nita, Forward scattering series and Padé approximants for acoustic wavefield propagation in a vertically varying medium, Communications in Computational Physics, 3(1)(2008)180 – 202.

[23] G.W. Peaceman, H.H. Rachford, The numerical solution of parabolic and elliptic differential equations, Journal of the society for industrial and applied mathematics, 3(1)(1955)28–41.

[24] G. R. Shubin, J. B. Bell, A modified equation approach to constructing fourth-order methods for acoustic wave propagation, SIAM J. Sci. Statits. Comput. 8(2)(1987)135–151.

[25] R. Shukla, X. Zhong, Derivation of high-order compact finite difference schemes for non-uniform grid using polynomial interpolation, Journal of Computational Physics, 204(2)(2005)404–429.

[26] P. Tong, D.H. Yang, B.L. Hua, High accuracy wave simulation - revised derivation, numerical analysis and testing of a nearly analytic integration discrete method for solving acoustic wave equation, International Journal of Solids and Structures, 48(2011) 56–70.

[27] Y. Wang, J. Zhang, Sixth order compact scheme combined with multi-grid method and extrapolation technique for 2D poisson equation, Journal of Computational Physics, 228(1)(2009)137–146.

[28] D.H. Yang, E. Liu, Z. J. Zhang, J.W. Teng, Finite-difference modelling in two-dimensional anisotropic media using a flux-corrected transport technique, Geophysical Journal International, 148(2)(2002) 320–328.

[29] D.H. Yang, J.M. Peng, M. Lu, T. Terlaky, Optimal nearly-analytic discrete approximation to the scalar wave equation, Bulletin of the Seismological Society of America, 96(3)(2006)1114–1130.

[30] D.H. Yang, G.J. Song, M. Lu, Optimal nearly-analytic discrete scheme for wave-filed simulation in 3D anisotropic media, Bulletin of the Seismological Society of America, 97(5)(2007)1557–1569.

[31] D.H. Yang, N. Wang, S. Chen, G.J. Song, An explicit method based on the implicit Runge-Kutta algorithm for solving the wave equations, Bulletin of the Seismological Society of America. 99(6)(2009) 3340–3354.

[32] D.H. Yang, L. Wang, A split-step algorithm with effectively suppressing the numerical dispersion for 3D seismic propagation modeling, Bulletin of the Seismological Society of America. 100(4)(2010)1470–1484.

[33] D.H. Yang., P. Tong, X.Y. Deng, A central difference method with low numerical dispersion for solving the scalar wave equation, Geophysical Prospecting, 60 (5)(2012) 885–905.

[34] D.H. Yang, N. Wang, and F.Q. Liu, A strong stability-preserving predictor-corrector method for seismic propagation simulations, Communications in Computational Physics. 12 (4)(2012)1006 –1032.

[35] D. You, A high-order Padé ADI method for unsteady convection-diffusion equations, Journal of Computational Physics, 214(2006) 1–11.

[36] W. Zhang, L. Tong, E. T. Chung, A new high accuracy locally one-dimensional scheme for the wave equation, Journal of Computational and Applied Mathematics, 236 (2011)1343–1353.